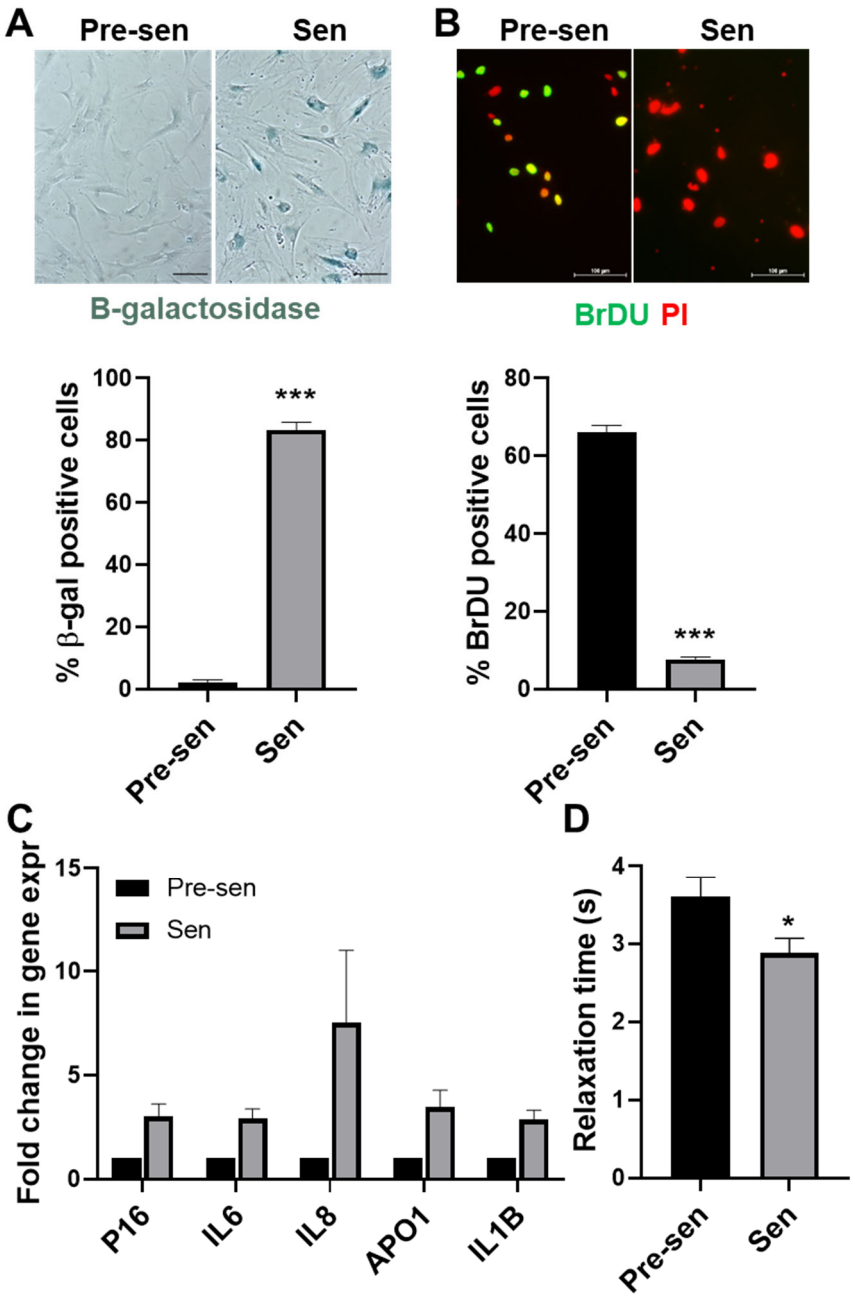

Figure S1. **(A-C) Characterization of radiation induced senescence and development of SASP in MSCs.** Staining and quantification of **(A)** SA-β-galactosidase (blue) and **(B)** BRDU (green: BrDU, red: propidium iodide) incorporation confirmed senescence in irradiated MSCs. **(C)** mRNA expression analysis by qRT-PCR for senescence markers (APO1, P16, IL6, IL8, IL1B); expression of all SASP markers was increased. **(D)** Quantification of average relaxation time (RT) for the nucleus signifying its transition into viscous domain showed significantly lower RT for senescent compared to pre-senescent MSCs. Student's t-tests were used to calculate statistical significance, and p-values less than 0.05 considered significant (*p<0.05, **p<0.01, ***p<0.001).

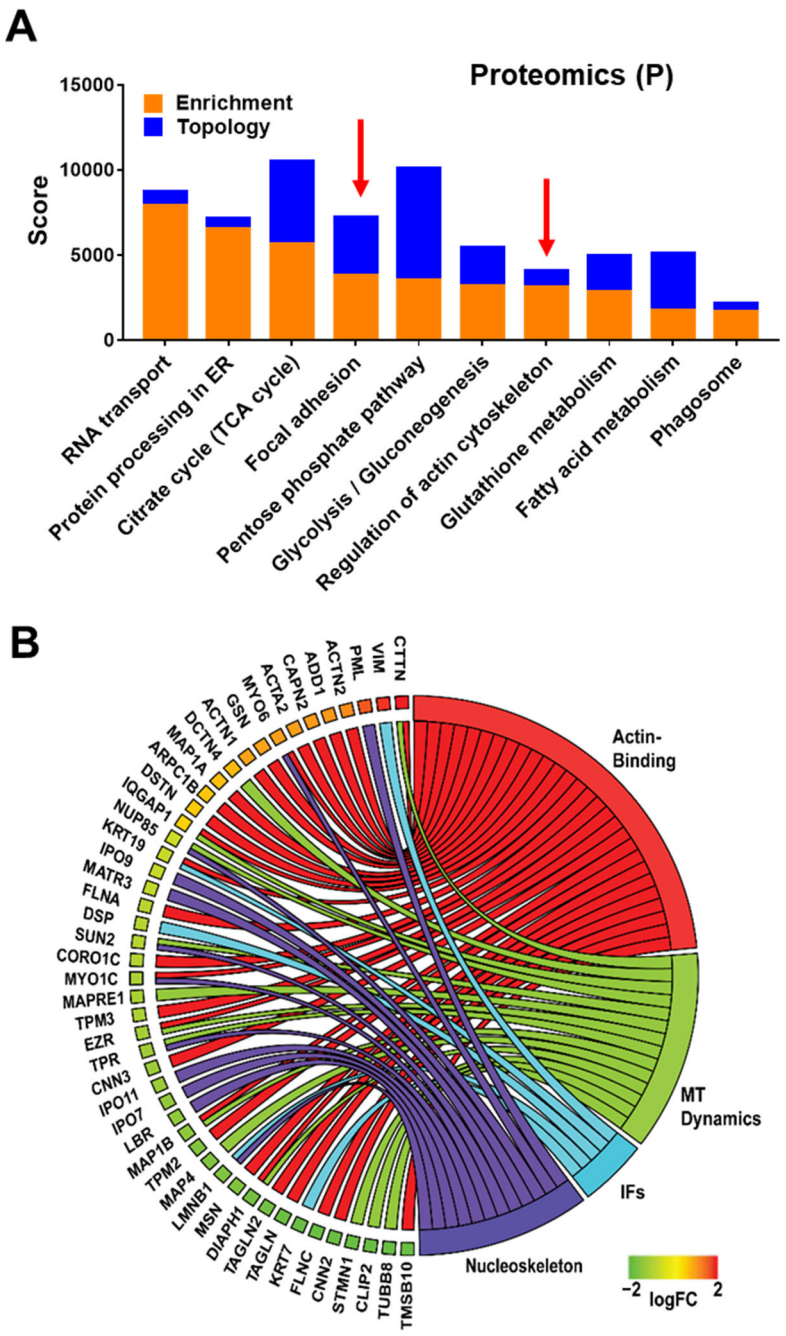

Protein	log2 FC
MCAM	-1.19
ALCAM	-0.83
ZYX	-2.99
ITGB1	0.51
VCL	0.59
ITGBL1	0.79
ITGB5	1.13
ITGA2	1.91

Protein	Log2FC
H2AFV	-1.96
H2AFZ	-2.22
H3F3A	-1.46
HDAC1	-0.92
HIST1H1B	-2.55
HIST1H1C	-3.27
HIST1H1E	-2.03
HIST1H1T	-3.29
HIST1H2BN	-3.00
HIST1H3D	-2.58
HIST1H4A	-1.94

Figure S2. **Pathway analysis of senescence induced changes in protein expression. (A)** Analysis of differentially regulated peptides showed enrichment for pathways including, focal adhesion, and actin cytoskeleton (red arrows). **(B)** GO chord plot of protein expression for senescent versus pre-senescent MSCs are reported for cytoskeleton and nucleoskeleton related proteins (FC-fold change, MT-Microtubule, IF-Intermediate filament). **(C)** Log2 FC in expression for genes related to adhesion and histone modification. **(D)** Western blot was used to analyze expression of LMNA and LMNB1 in senescent MSCs. While LMNA expression was upregulated, LMNB1 was downregulated in senescent MSCs compared to pre-senescent cells.

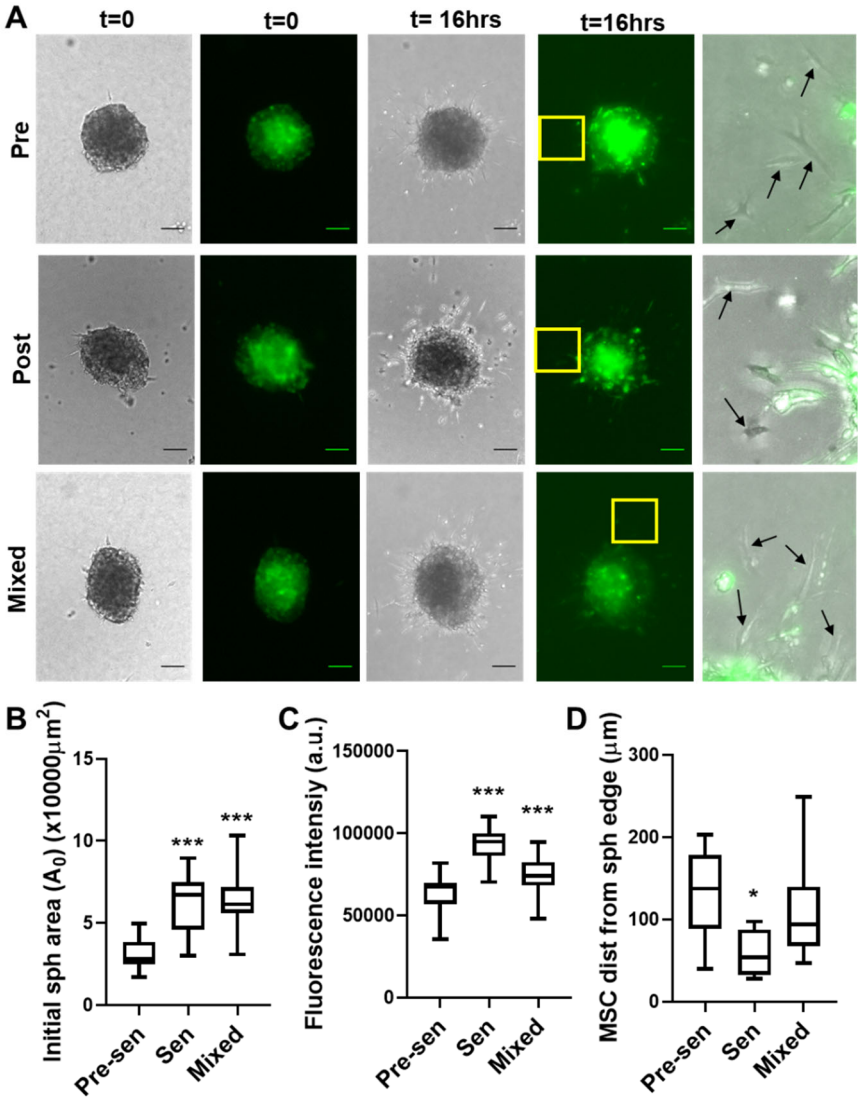

Figure S3. **Comparative role of pre-senescent and senescent MSCs in BCC invasion in 3D collagen gels. (A)** Time-lapsed imaging was used to monitor BCC invasion over 16 hours from spheroids formed with equal numbers of GFP negative MSCs and GFP positive MDA-MB-231 cells and embedded in 1.5 mg/ml collagen gels (Scale bar 100 um). Pre-senescent and senescent MSCs were also combined at 1:1 ratio (mixed). **(B-C)** Initial area (A_0) of the embedded spheroids (**B**) and fluorescence measurement of GFP positive MDA-MB-231 cells (measured with plate reader) (**C**) were quantified to assess the number of BCCs. Presence of senescent cells resulted in spheroids with larger initial area and higher number of BCCs. **(D)** To assess the role of MSCs in invasion, we quantified the invaded distance of MSCs from spheroid boundary. This confirms that pre-senescent MSCs move further from spheroid surface than senescent MSCs. Student's t-tests were used to calculate statistical significance, and p-values less than 0.05 considered significant (*$p < 0.05$, **$p < 0.01$, ***$p < 0.001$).

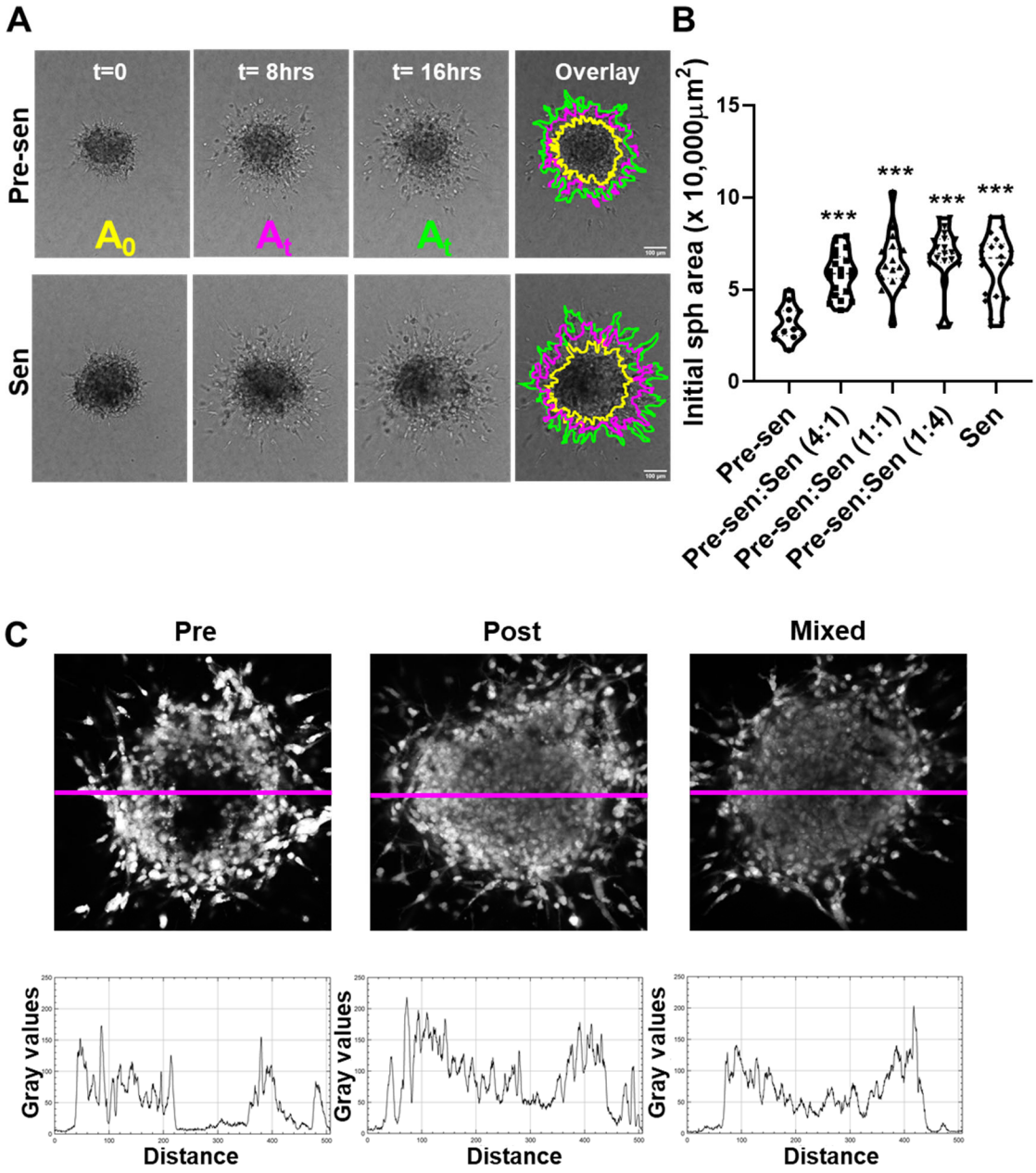

Figure S4. **Role of pre-senescent and senescent MSCs in organization of spheroid and invasion. (A)** Time-lapsed imaging was used to monitor cell migration from spheroids using matrix interface model. Images of spheroid migration over time with regions highlighted in yellow, magenta and green depict the area at times, t= 0, 8 and 16 hours, respectively **(scale bar = 100 μm)**. **(B)** Spheroid area was analyzed for MDA-MB-231 cell spheroids cultured with both individual and mixed population of pre-senescent and senescent MSCs embedded in collagen gels. For the mixed populations, the ratio between MSCs were varied between 4:1 to 1:4. The presence of senescent MSCs increased spheroid size for all ratios compared to spheroids with only pre-senescent MSCs. **(C)** Images from multiphoton confocal microscopy were used to determine cell density distribution in 3D spheroids. The gray intensity representing cell distribution across the central axis (magenta) of the spheroid core was plotted in ImageJ to look at differences in cell density at spheroid core.

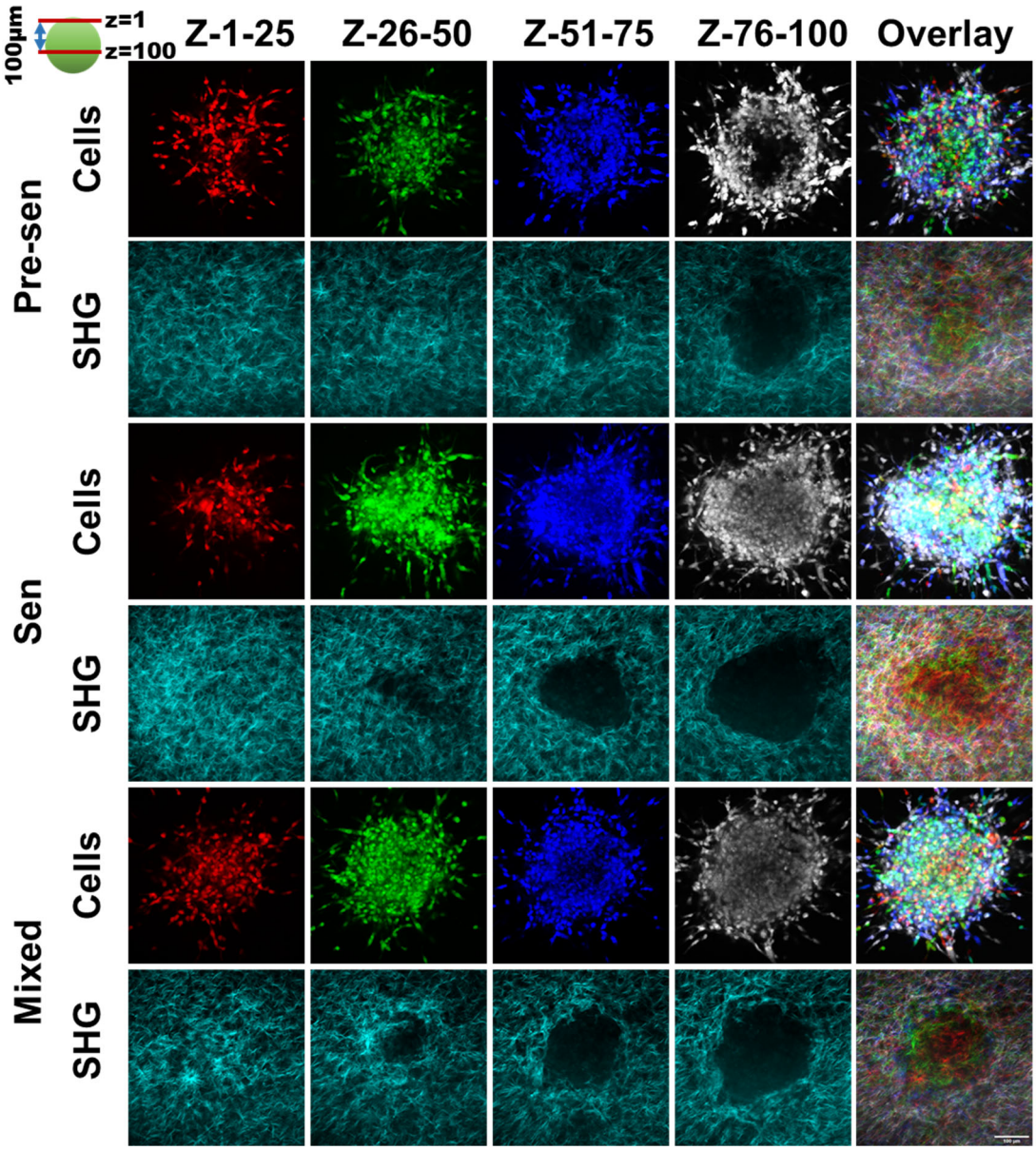

Figure S5. **SHG analysis of collagen structure surrounding spheroids.** Spheroids embedded in collagen gels were imaged by multiphoton microscopy using second harmonic generation to identify collagen (shown in **cyan**) and NucRed to identify cells. Cell z-stacks were color coded (*red: z1-25, green: z26- 50, blue: z51-75, gray: z76-100*) to distinguish different sections of the spheroid **(scale bar=100µm)**. Mosaic images (overlay) of the color-coded sections highlight packing density of spheroids, which is increased for spheroids co-cultured with senescent MSCs.

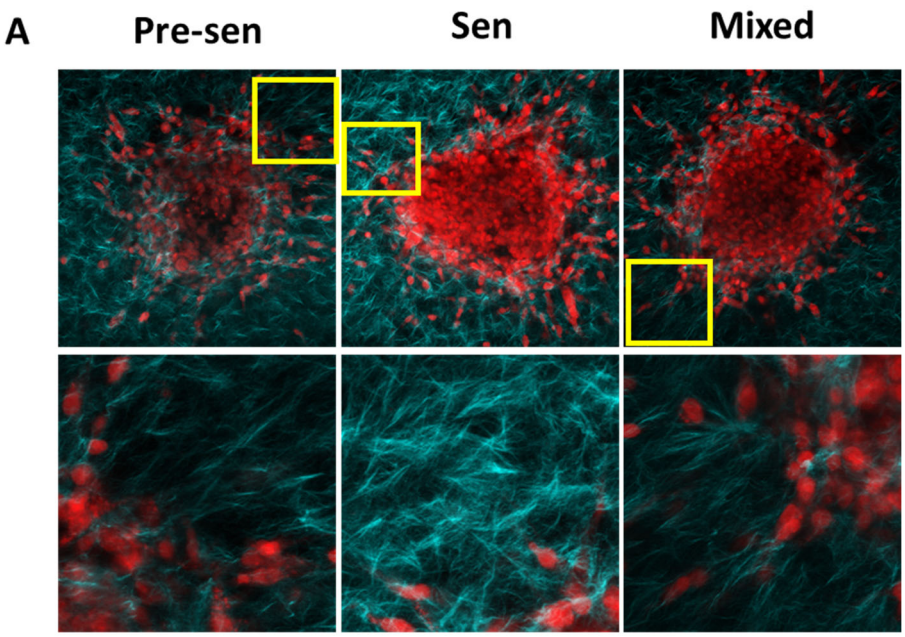

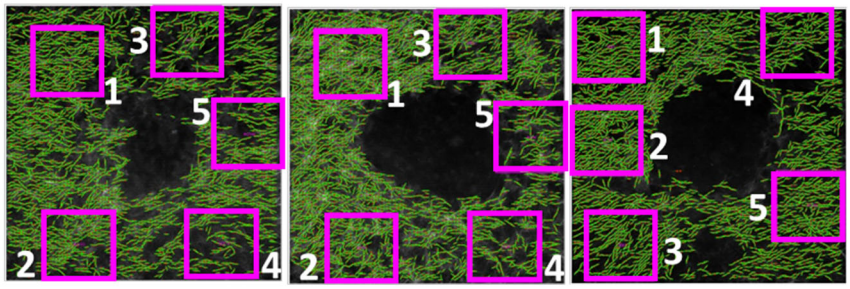

C

ROI label	Align-ment	Box density
ROI1	0.74	84.66
ROI2	0.69	72.79
ROI3	0.61	50.22
ROI4	0.7	46.39
ROI5	0.87	62.11
AVG	0.72	63.23
CV	0.12	0.22
Overall AVG	0.74	63.67

ROI label	Align-ment	Box density
ROI1	0.67	92.56
ROI2	0.48	74.83
ROI3	0.76	65.13
ROI4	0.55	53.42
ROI5	0.73	52.3
AVG	0.64	67.65
CV	0.17	0.22
Overall AVG	0.64	70.2

ROI label	Align-ment	Box density
ROI1	0.77	82.75
ROI2	0.67	85.11
ROI3	0.7	75.61
ROI4	0.67	65.1
ROI5	0.69	75.91
AVG	0.70	76.9
CV	0.05	0.09
Overall AVG	0.69	62.43

Figure S6. **Analysis of local and global structure surrounding spheroids using CT-FIRE.** (**A**) Spheroids embedded in collagen gels were imaged by multiphoton microscopy using second harmonic generation to identify collagen (shown in **cyan**) and NucRed to identify cells (shown in **red**); images include average intensity projections of z-stack and 2D slice for region highlighted by yellow box. (**B-C**) The structure of collagen around the embedded spheroid was analyzed using CurveAlign ROI analysis. For each image, 5 rectangular boxes were selected around the primary spheroid to quantify co-efficient of alignment. Properties of the ROIs along with the overall image are reported here.

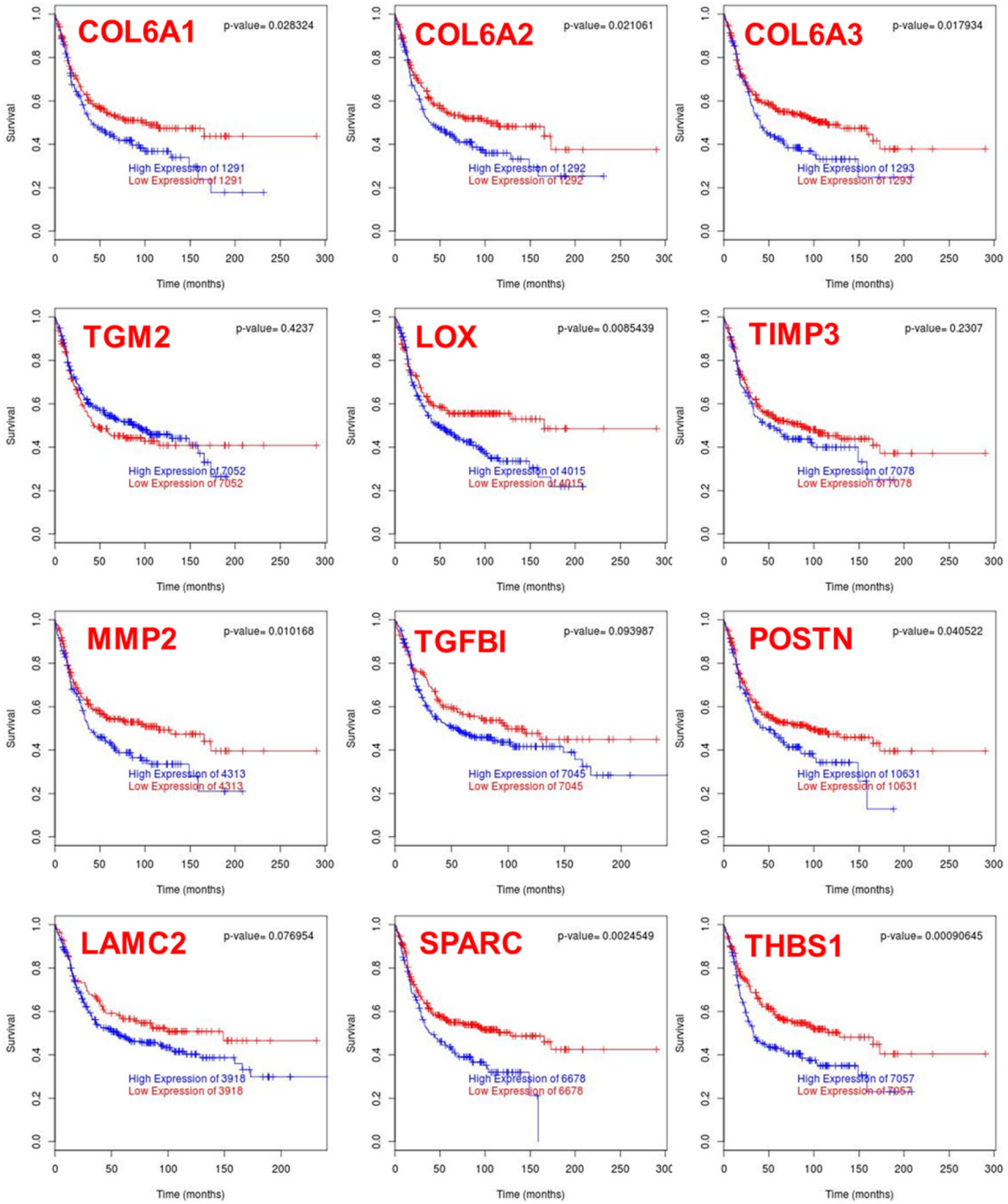

Figure S7. **Survival analysis of senescent associated ECM signature in breast cancer.** ECM signature from senescent MSCs was used to analyze Kaplan-Meier estimates of disease-free survival for breast cancer using free online tool BreastMark at http://glados.ucd.ie/BreastMark/index.html**.** ECM genes upregulated in senescent MSCs including, expression of collagen isoforms (COL6A1, COL6A2, COL6A3), matrix modifying enzymes (LOX, MMP2), and matricellular proteins (POSTN, THBS1, SPARC) are correlated with poor prognosis in basal subtype of breast cancer ($p<0.05$).